# Perhalogenated Anions as Structure Directing Agents of Cationic Coordination Polymers

Kevin C. Lofgren, Kellii J. Fusari, Daniel G. Droege, Jeremy L. Barnett, Timothy C. Johnstone and Scott R. J. Oliver\*

Department of Chemistry and Biochemistry, University of California, Santa Cruz, California 95064, United States *Trifluoroacetate, trichloroacetate, tribromoacetate, triiodoacetate, perhalogenated acetate, anion exchange, CP, halogenated pollutants* 

**ABSTRACT**: We investigate the synthesis of coordination polymers (CPs) comprising silver cations, 4,4'-bipyridine and the charge-balancing perhalogenated acetate anions trifluoroacetate (CF<sub>3</sub>COO<sup>-</sup>), trichloroacetate (CCl<sub>3</sub>COO<sup>-</sup>), tribromoacetate (CBr<sub>3</sub>COO<sup>-</sup>) or triiodoacetate (CI<sub>3</sub>COO<sup>-</sup>). The syntheses involved anion exchange using the starting CP silver 4,4'-bipyridine acetate. Multianalytical characterization was conducted using powder X-ray diffraction, single crystal X-ray diffraction, optical microscopy and thermogravimetric analysis. Our findings revealed that CPs were formed with CF<sub>3</sub>COO<sup>-</sup> or CCl<sub>3</sub>COO<sup>-</sup> as the charge-balancing anion and exhibited notable stability. In contrast, reactions with CBr<sub>3</sub>COO<sup>-</sup> and CI<sub>3</sub>COO<sup>-</sup> showed that the starting anion undergoes decomposition to bromide, iodide or triiodide before being incorporated into the resulting material. This study sheds light on the interactions between perhalogenated anions and CPs and the potential for the use of CPs in the removal of perhalogenated "forever chemicals."

#### INTRODUCTION

In recent years, the field of CPs has witnessed significant advancements, offering a versatile platform for the design of novel materials with diverse potential applications. Among these, cationic metal-organic frameworks (CPs) have emerged as promising candidates for the selective adsorption of environmental pollutants through anion exchange reactions.<sup>1,2</sup> Only a limited number of studies, however, have been dedicated to CPs containing perhalogenated anions. In this study, perfluoro-, perchloro-, perbromo- and periodoacetate anions were strategically chosen due to their relevance as environmental pollutants, with many haloacetates being of human concern due to their carcinogenic nature.<sup>3–5</sup> From the perspective of the fundamental chemistry of reticular materials, the perhalogenated acetates comprise a family of uninvestigated anionic structure-directing agents for CPs. These compounds find their way into the environment through anthropogenic processes, putting pressure on the need to discover materials that can remediate these pollutants. For example, chlorination is widely implemented for drinking water disinfection, but this process can unintentionally produce chlorinated haloacids through reactions of chlorine and natural organic matter. This problem becomes exceptionally more serious in regions implementing seawater for sanitation such as Hong Kong, since the resulting wastewater can have high concentrations of bromide (20-31 µg/L) and iodide (30-60 μg/L) that can react with organic matter to form toxic haloacids.<sup>6,7</sup> Disinfection of this wastewater produces an increased concentration of chlorinated and iodinated haloacids such as CCl<sub>3</sub>COOH and CI<sub>3</sub>COOH. <sup>8,9</sup> Due to their low pK<sub>a</sub> values, these species will form CCl<sub>3</sub>COO<sup>-</sup> and CBr<sub>3</sub>COO<sup>-</sup> under ambient conditions.

The United States Environmental Protection Agency regulates five haloacetic acids (HAAs) in drinking water, including CCl<sub>3</sub>COOH. CCl<sub>3</sub>COO<sup>-</sup> was a once widely used as a potent herbicide due to its phytotoxicity. <sup>10</sup> CCl<sub>3</sub>COO<sup>-</sup> can also be formed through various processes, such as photolysis of chlorinated hydrocarbons in ambient air, microbial processes in plants and soils and through the chlorination of wastewater. <sup>11</sup>

Other regulated HAAs include chloroacetic acid, bromoacetic acid, dichloroacetic acid and dibromoacetic acid. <sup>12</sup> On the other hand, CBr<sub>3</sub>COOH is a monitored compound in the 4th Unregulated Contaminate Monitoring Rule (UCMR4) along with bromodichloroacetic acid, bromochloroacetic acid and chlorodibromoacetic acid. <sup>3</sup> Both the known and potential health hazards of these compounds put pressure on developing technology for their efficient removal. The use of CPs for the trapping of haloacetates has an advantage over other methods such as photochemical, <sup>13,14</sup> electrochemical, <sup>15–17</sup> zero-valent metal <sup>18,19</sup> and biodegredation <sup>20–22</sup> methods since the halogens are removed from the system and not simply converted to other forms.

Additionally, trifluoroacetic acid (CF<sub>3</sub>COOH) has been receiving significant attention due to its polluting nature and resistance to decomposition.<sup>23–25</sup> Unlike other haloacids, CF<sub>3</sub>COOH isn't susceptible to breakdown by chemical, physical, biological or photochemical processes, resulting in environmental accumulation.<sup>26–28</sup> Primary sources of CF<sub>3</sub>COOH originate from degradation of chlorofluorocarbons in the atmosnotably HCFC-134a (CF<sub>3</sub>CH<sub>2</sub>Cl), HCFC-124 (CF<sub>3</sub>CHFCl) and HCFC-123 (CF<sub>3</sub>CHCl<sub>2</sub>), as well as through the decomposition of fluorinated compounds from industrial and other high-temperature applications. 29 The Chinese fluorochemical industry is a major producer of CF<sub>3</sub>COOH through their intentional and unintentional emission of fluorine-containing gases.<sup>30</sup> While CF<sub>3</sub>COOH is typically present in the environment at levels too low to be a concern to human health, its inability to be broken down by reductive or oxidative processes will ensure its accumulation and should therefore be of concern.

In this study, we present a comprehensive exploration of the interactions between the CP silver 4,4'-bipyridine acetate, {[(Ag)(4,4'-bipyridine)][CH<sub>3</sub>COO]}, denoted as SBA, and the perhalogenated anions perfluoro-, perchloro-, perbromo- and periodoacetate. This study furthers our understanding of the structural modifications induced by the anion exchange process of perhalogenated anions and the reactivity of perhalogenated acetates.

#### **EXPERIMENTAL**

## Reagents

Silver acetate (CH<sub>3</sub>COOAg, Fisher Chemical, 98%), 4,4'-bipyridine [(NC<sub>5</sub>H<sub>4</sub>)<sub>2</sub>, Acros Organics, 98%], sodium trifluoroacetate (CF<sub>3</sub>COONa, ThermoScientific, 98%), sodium trichloroacetate (CCl<sub>3</sub>COONa, Oakwood Chemical), tribromoacetic acid (CBr<sub>3</sub>COOH, Sigma-Aldrich, 99%) and sodium triiodoacetate (CI<sub>3</sub>COONa, Combi-Blocks, 95%) were used as-received without further purification. The water used for all synthesis and exchange was obtained from a Millipore water purification system.

#### Instrumentation

Powder X-ray diffraction (PXRD) was measured on a Rigaku Americas Miniflex Plus diffractometer, with a scan rate of 2°/min and a 0.04° step size using 13 kV, 15 mA Cu K $\alpha$  radiation ( $\lambda = 1.5418$  Å). Singe crystal X-ray diffraction (SCXRD) was performed by mounting single crystals on a MiTeGen polyimide loop and cooled to 100 K on a Rigaku Synergy-S X-ray diffractometer. Diffraction of Cu Kα radiation from a PhotonJet-S microfocus source was detected using a HyPix-6000HE hybrid photon counting detector. Screening, indexing, data collection and data processing were performed with CrysAlispro.31 The structure was solved using SHELXT and refined using SHELXL following established strategies.<sup>32–34</sup> All non-H atoms were refined anisotropically. FTIR was measured on a PerkinElmer Spectrum One spectrophotometer with KBr pellets. Thermogravimetric analysis (TGA) studies were performed using a TA Instruments Q500 TGA, heating from 25 to 550 °C under an N2 purge and a gradient of 5 °C/min. In situ variable temperature PXRD was performed on a Rigaku SmartLab X-ray Diffractometer with Cu K $\alpha$  radiation ( $\lambda = 1.5418$  Å) in parallel beam geometry from  $2^{\circ}$  to  $50^{\circ}$  ( $2\theta$ ) at a scan rate of  $2^{\circ}$ /min and  $0.02^{\circ}$  step size.

# Synthesis of SBA

SBA was synthesized using a previously reported method. A microcrystalline powder with a blade morphology approximately  $1.5 \times 0.08 \ \mu m^2$  in size was synthesized at room temperature. In a typical synthesis, silver acetate (0.10 g, 0.6 mmol) was combined with 4,4′-bipyridine (0.10 g, 0.64 mmol) and water (10 mL) and gently stirred in a covered beaker for 1 h. The powder was then collected via vacuum filtration and rinsed with deionized water and acetone to aid in drying (yield: 0.19 g, 99% based on silver acetate).

# Synthesis of SB(CF<sub>3</sub>COO<sup>-</sup>)

Previously synthesized SBA (0.10 g, 0.29 mmol) was added to water (10 mL) in a 100 mL beaker equipped with a stir bar. To this mixture, CF<sub>3</sub>COONa (0.018 g, 0.13 mmol) was added and the mixture was allowed to stir for 1 h at room temperature. The resulting white solid (0.10 g, 98% yield) was collected *via* vacuum filtration and rinsed with water followed by acetone to aid in the drying process. Crystals of the resulting CP silver 4,4′-bipyridine trifluoroacetate [SB(CF<sub>3</sub>COO<sup>-</sup>), which we denote as SLUG-59, for University of California, Santa Cruz, Structure No. 59] suitable for SCXRD were obtained by adding freshly synthesized SB(CF<sub>3</sub>COO<sup>-</sup>) (0.0330 g) to water (10 mL) in a 15 mL Teflon lined autoclave with heating at 150 °C for 2 d followed by slow cooling at a rate of 0.1 °C/min.

# Synthesis of SB(CCl<sub>3</sub>COO<sup>-</sup>)

Previously synthesized SBA (0.10 g, 0.29 mmol) was added to water (10 mL) in a 100 mL beaker equipped with a stir bar. To this mixture, CCl<sub>3</sub>COONa (0.024 g, 0.13 mmol) was added and the mixture was allowed to stir for 1 h at room temperature. The resulting white solid (0.10 g, 99% yield) was collected *via* vacuum filtration and rinsed with water followed by acetone to aid in the drying process. Single crystals

of the resulting CP silver 4,4'-bipyridine trichloroacetate [SB(CCl<sub>3</sub>COO<sup>-</sup>), which we denote as SLUG-60] were obtained by dissolving SB(CCl<sub>3</sub>COO<sup>-</sup>) ( $\sim$  10 mg) in a few mL of concentrated ammonia. The undissolved solid was removed by filtration using a syringe fitted with a filter and the saturated SB(CCl<sub>3</sub>COO<sup>-</sup>) ammonia solution was placed in a small glass vial. The vial was covered with Parafilm and one small hole was made in the film using a toothpick to allow for slow ammonia evaporation.

## Reaction of SBA with CBr<sub>3</sub>COO

Due to difficulties with finding a commercial source of CBr<sub>3</sub>COONa, the acid form, CBr<sub>3</sub>COOH, was used instead. To a 100 mL beaker, water (8 mL) was added followed by the addition of CBr<sub>3</sub>COOH (0.077 g, 0.26 mmol) with stirring. The CBr<sub>3</sub>COOH was converted to CBr<sub>3</sub>COONa using 0.1 M NaOH (2.6 mL). To this solution, previously synthesized SBA (0.10 g, 0.29 mmol) was then added and allowed to stir for 1 h. The resulting white solid was collected via vacuum filtration and rinsed with water followed by acetone to aid in the drying process. Both 1:1 and 2:1 (CBr<sub>3</sub>COONa:SBA) mole ratios were used in both light and dark environments to avoid any photochemical reaction of tribromoacetate. All bulk products gave the same experimental PXRD pattern, which differed from the theoretical pattern obtained from SCXRD data of a CP (which we denote as SLUG-61) from this reaction. These crystals were obtained by dissolving approximately 10 mg of freshly synthesized material in a few mL of concentrated ammonia. The undissolved solid was filtered off using a syringe filter and the saturated CP ammonia solution was placed in a small glass vial. The vial was covered with Parafilm and one small hole was made in the film using a toothpick to allow for slow ammonia evaporation.

## Reaction of SBA with CI<sub>3</sub>COONa

All steps were performed in the dark to avoid any photochemical reactions of triiodoacetate. Previously synthesized SBA (0.10 g, 0.29 mmol) was added to water (10 mL) in a 15 mL Teflon lined autoclave. To this mixture, CI<sub>3</sub>COONa (0.054 g, 0.26 mmol) was added and mixed by inverting the autoclave several times. The mixture was then heated at 150 °C for 3 d and cooled to room temperature at a rate of 0.1 °C/min. The crimson red crystals were collected *via* vacuum filtration and rinsed with water followed by acetone to aid in the drying process. These crystals were suitable for SCXRD (the structure we denote as SLUG-62). The experimental PXRD pattern of the bulk product did not match the theoretical pattern obtained through SCXRD.

#### RESULTS AND DISCUSSION

## SBA Anion Exchange with CF<sub>3</sub>COO<sup>-</sup>

CF<sub>3</sub>COO<sup>-</sup> undergoes anion exchange with our previously reported CP, silver 4,4'-bipyridine acetate {[(Ag)(4,4'-bipyridine)][(CH<sub>3</sub>COO)], denoted as SBA}.<sup>35,36</sup> Anion exchange is a highly desirable property of CPs made possible by the loosely coordinated crystallographic anions oriented within the CP.<sup>37-39</sup> The anion exchange process is solvent mediated and involves the breaking apart of the original CP and the release of the starting anion (acetate) into solution. Reformation of the CP around the new incoming anion (CF<sub>3</sub>COO<sup>-</sup>) then occurs.<sup>40</sup> The preference of a CP for one anion over another is due in part to the solubility of the anions in question.<sup>36</sup> With an appropriately selected starting CP, the harmful anion will be less soluble than that originally present and it will be more energetically favorable for the pollutant to reside within the CP than for it to remain in solution.

We have previously disclosed the crystal structure of SBA,<sup>35</sup> but certain aspect of this structure merit discussion to facilitate

comparison to the following structures that we will describe. SBA crystalizes in space group  $P2_1/c$  and consists of polymeric chains of  $Ag^+$  coordinated to 4,4'-bipyridine (Figure 1). The charge balancing acetate anions are weakly bound to  $Ag^+$  and sandwiched between the  $\pi$ -stacked polymeric chains. <sup>35</sup> The ions of  $Ag^+$  in neighboring chains are colinear and arranged into dimers with a  $Ag^-$  Ag distance of 3.1347(8) Å. <sup>35</sup> The charge balancing acetates form  $\mu_2$  bridges with two  $Ag^+$  cations of adjacent polymeric chains. Occupational disorder is observed among the 4,4'-bipyridine units (Figure 1); the disorder arises from rocking of the pyridine rings, which are anchored at the nitrogen and para carbon atoms. The structure contains six water molecules in the asymmetric unit that occupy the space between silver complex chains and form an extensive hydrogen bonding network. <sup>35</sup>

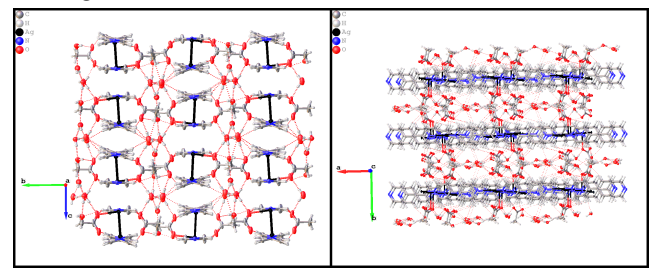


**Figure 1.** Crystal structure for the starting material SBA, showing acetate sandwiched between polymeric chains of 4,4'-bipyridine and  $Ag^+$ , with bipyridine  $\alpha$  and  $\beta$  carbon disorder and crystallographic waters present. Left image: view down the *a*-axis, with polymeric chains extending in and out of the page; right image: view down the *c*-axis showing the polymeric chains stacked on top of one another in the plane of the page.

It was discovered that SBA can sequester CF<sub>3</sub>COO<sup>-</sup> from water while releasing benign acetate via an anion exchange process. The lower solubility of CF<sub>3</sub>COO<sup>-</sup> compared to acetate encourages a quick and successful exchange, resulting in the novel  $\{(Ag)(4,4'-bipyridine)\}[CF_3COO],$ CP denoted SB(CF<sub>3</sub>COO<sup>-</sup>); ORTEP diagram **Figure S1**; optical micrograph Figure S2}. The differences in the solubility of CH<sub>3</sub>COO<sup>-</sup> and CF<sub>3</sub>COO<sup>-</sup> arises from their different free energies of solvation. 41,42 While it is true the electronegativity of fluorine potentially makes for a more favorable dipole interaction with water than hydrogen, the larger atomic radius of fluorine requires more water molecules to orient themselves into a solvation sphere than is required for hydrogen. This decrease in entropy due to a larger solvation sphere for CF<sub>3</sub>COO<sup>-</sup> is more significant than the stronger dipole interactions with water. The effect of fluorine on the solubility of organic molecules is well reported.<sup>43</sup> The resulting SB(CF<sub>3</sub>COO<sup>-</sup>) was stable enough that when 10x molar excess potassium acetate (KOAc) was introduced to SB(CF<sub>3</sub>COO<sup>-</sup>) in water, the starting SBA could not be regenerated.

SB(CF<sub>3</sub>COO<sup>-</sup>) crystallizes in space group Pnc2 (**Figure 2**) and consists of positively charged polymeric chains of  $Ag^+$  and 4,4'-bipyridine. The chains stack on top of one another with a nearest centroid<sub>pyridine</sub>-to-centroid<sub>pyridine</sub> distance of 3.540(9) Å. Charge balancing CF<sub>3</sub>COO<sup>-</sup> ions reside between the  $\pi$ -stacked layers and colinear cations of  $Ag^+$  are arranged into dimers with a  $Ag\cdots Ag$  distance of 3.2304(12) Å. This layout once again reduces the  $\pi$ -stacking of adjacent bipyridine molecules but increases the stability of the framework through covalent argentophilic connectivity and forms a structure similar to that of the

starting SBA. The PXRD of bulk SB(CF<sub>3</sub>COO<sup>-</sup>) obtained through the anion exchange reaction of SBA with CF<sub>3</sub>COO<sup>-</sup> matched the theoretical spectrum obtained from SCXRD (**Figure 3**). Also shown in Figure 3 is the experimental PXRD pattern for the starting SBA to emphasize the successful anion exchange. IR spectroscopy was employed to further characterize the anion exchange process with new peaks and shifts in peaks being the result of the replacement of CH<sub>3</sub>COO<sup>-</sup> for CF<sub>3</sub>COO<sup>-</sup> (Figure S3).

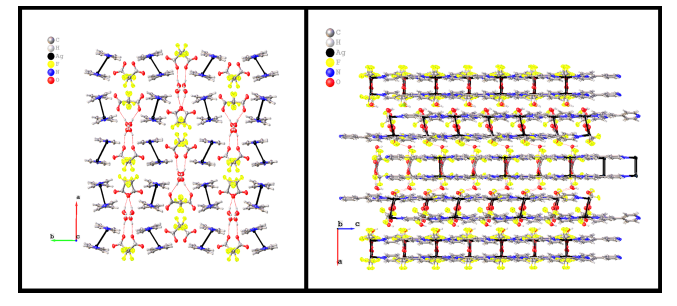


**Figure 2.** The crystal structure of SB(CF<sub>3</sub>COO<sup>-</sup>), showing charge balancing CF<sub>3</sub>COO<sup>-</sup> and crystallographic water sandwiched between polymetric chains of Ag<sup>+</sup> and 4,4'-bipyridine. Left image: view down the c-axis with polymeric chains propagating in and out of the page; right image: view down the b-axis showing the polymeric chains stacked on top of one another.

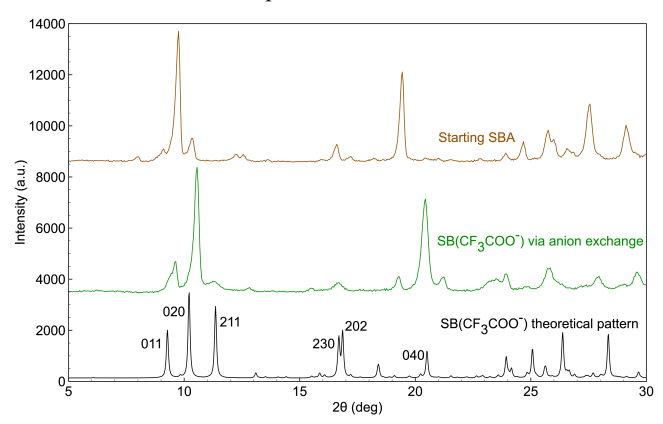


**Figure 3.** PXRD spectra for SB(CF<sub>3</sub>COO<sup>-</sup>), showing the theoretical pattern obtained from SCXRD data (black) with Miller indices of majority peaks and the experimental pattern (green) obtained from bulk SB(CF<sub>3</sub>COO<sup>-</sup>) synthesized *via* aqueous anion exchange between SBA (also included as top pattern for comparison, brown) and CF<sub>3</sub>COO<sup>-</sup>.

Solubility studies of SB(CF<sub>3</sub>COO<sup>-</sup>) were also performed using ICP-OES with filtered, saturated aqueous solutions of SB(CF<sub>3</sub>COO<sup>-</sup>) and SBA. It was determined that a saturated solution of SB(CF<sub>3</sub>COO<sup>-</sup>) prepared over 3 d under ambient conditions contains 3.2 μM Ag<sup>+</sup>. The solvated silver results from the framework partially dissociating. Saturated solutions of the starting material SBA had a silver concentration of 5.0 μM. The lower solubility of SB(CF<sub>3</sub>COO<sup>-</sup>) as compared to SBA is partly responsible for the successful aqueous anion exchange between SBA and CF<sub>3</sub>COO<sup>-</sup>. The SBA dissociates, releasing the more soluble acetate anion while the less soluble CF<sub>3</sub>COO<sup>-</sup> is taken up, forming a SB(CF<sub>3</sub>COO<sup>-</sup>) suspension. Furthermore, PXRD and IR spectroscopy were used to show that SB(CF<sub>3</sub>COO<sup>-</sup>) was stable over the course of six months when stored dry under normal laboratory conditions (**Figure 4**). This was shown by

observing there were negligible changes to the PXRD or FTIR pattern. The thermal stability of the material was also explored and TGA showed the solid material is stable to ca. 210 °C in air at atmospheric pressure (**Figure S4**). Variable-temperature PXRD confirmed this mass loss event is due to the decomposition of the material to an amorphous product (**Figure S5**). The peak at  $2\theta \sim 38^\circ$  arises from the sample holder. This is a significantly higher decomposition temperature than that of SBA, which showed its major mass loss around  $140^\circ \text{C}$ .

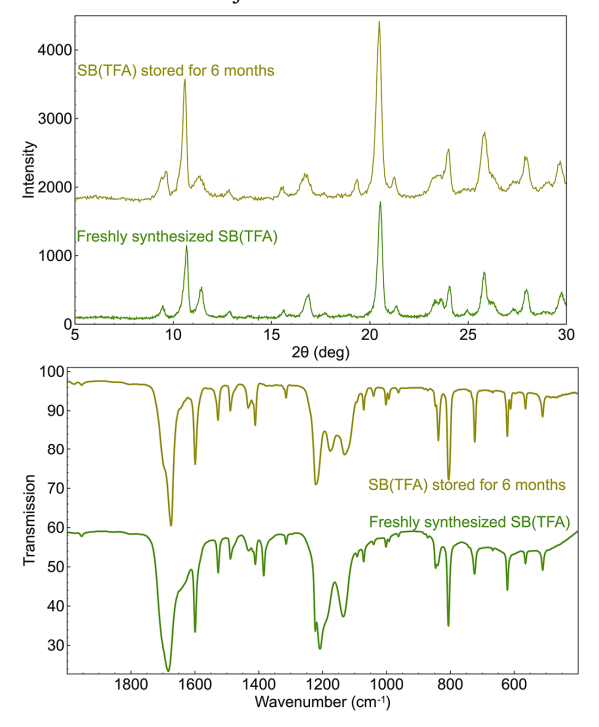


**Figure 4.** PXRD and FTIR (inset) of SB(CF<sub>3</sub>COO<sup>-</sup>), showing that the material is stable over the course of six months when stored in a vial under normal laboratory conditions.

# SBA Anion Exchange with CCl<sub>3</sub>COO<sup>-</sup>

SBA also demonstrated an ability to sequester CCl<sub>3</sub>COO-, forming the CP {[(Ag)(4,4'-bipyridine)][CCl<sub>3</sub>COO], represented as SB(CCl<sub>3</sub>COO<sup>-</sup>); ORTEP diagram: Figure S6; optical micrograph: Figure S7}. As was seen for SB(CF<sub>3</sub>COO<sup>-</sup>), the resultant exchange product of SBA with CCl<sub>3</sub>COO<sup>-</sup> is a onedimensional CP, characterized by polymeric chains of Ag<sup>+</sup> and 4,4'-bipyridine, similar in structure to SBA and SB(CF<sub>3</sub>COO<sup>-</sup>); the nearest centroid<sub>pyridine</sub>-to-centroid<sub>pyridine</sub> distance is 4.0508(18) Å. CCl<sub>3</sub>COO<sup>-</sup> is loosely bound between the polymeric chains, forming a framework with P2<sub>1</sub>/c symmetry (Fig**ure 5**). FTIR allows the exchange to be followed as new peaks associated with CCl<sub>3</sub>COO<sup>-</sup> emerged (Figure S8). Unlike SB(CF<sub>3</sub>COO<sup>-</sup>), the Ag<sup>+</sup> cations do not dimerize and the 4,4'-bipyridine organic linkers do not engage in  $\pi$ -stacking, likely due to the larger size of the anion. The theoretical PXRD of SB(CCl<sub>3</sub>COO<sup>-</sup>) obtained through SCXRD matched the experimental pattern obtained via anion exchange of CCl<sub>3</sub>COO<sup>-</sup> with SBA (Figure 6).

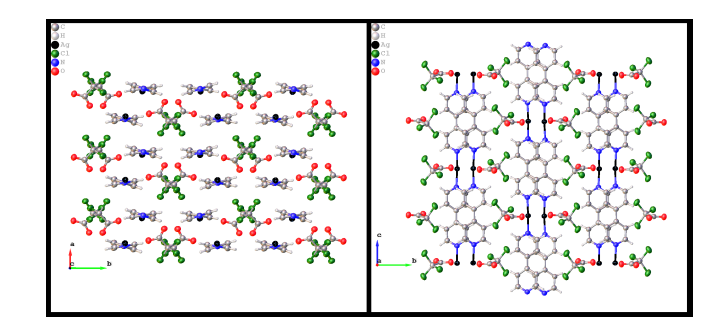


**Figure 5.** The crystal structure of SB(CCl<sub>3</sub>COO<sup>-</sup>), obtained through anion exchange of SBA with CCl<sub>3</sub>COONa. Right image: view down the *c*-axis with polymeric chains extending in and out of the page; left image: view down the *a*-axis, showing polymeric chains stacked upon one another.

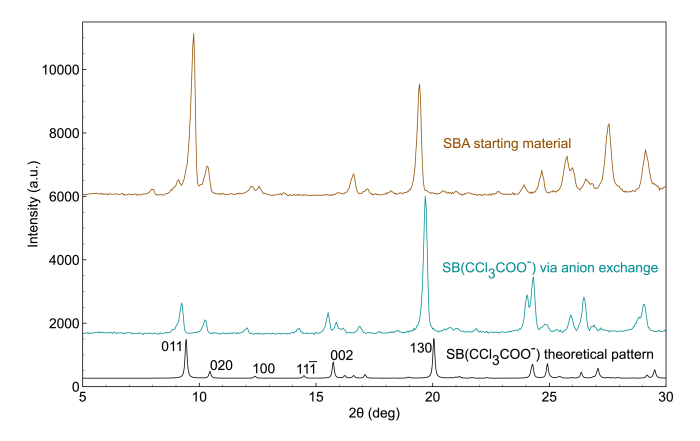


**Figure 6.** PXRD spectra for SB(CCl<sub>3</sub>COO<sup>-</sup>), showing the theoretical pattern obtained from SCXRD data (black) with Miller indices of major peaks and the experimental pattern (blue) obtained from SB(CCl<sub>3</sub>COO<sup>-</sup>), synthesized *via* aqueous anion exchange between SBA (also included as top pattern for comparison, brown) and CCl<sub>3</sub>COO<sup>-</sup>.

Since the structure of SB(CCl<sub>3</sub>COO<sup>-</sup>) doesn't engage in  $\pi$ stacking or silver dimerization like SB(CF<sub>3</sub>COO<sup>-</sup>) or SBA, one might expect SB(CCl<sub>3</sub>COO<sup>-</sup>) to be more soluble in water due to the lack of these structurally stabilizing interactions. It was determined, however, that filtered, saturated mixtures of SB(CCl<sub>3</sub>COO<sup>-</sup>) had an Ag<sup>+</sup> concentration of 1.8 μM, the lowest value of the frameworks explored thus far. The solubility trend is  $SB(CCl_3COO^-) < SB(CF_3COO^-) < SBA (1.8 < 3.2 < 5.0 \mu M)$ and follows expectation based on anion solubility. CCl<sub>3</sub>COOwould be expected to be less soluble than CF<sub>3</sub>COO<sup>-</sup> due to its larger size and lower electronegativity. This is because CCl<sub>3</sub>COO<sup>-</sup> would require a larger solvation sphere and the dipole interactions with water would be less favorable than for CF<sub>3</sub>COO<sup>-</sup> and in turn acetate for reasons mentioned previously. This aspect underscores the potential of these types of CPs to selectively trap harmful chlorinated organic anions. As was the case with SB(CF<sub>3</sub>COO<sup>-</sup>), when 10x molar excess KOAc was introduced to a mixture of SB(CCl<sub>3</sub>COO<sup>-</sup>) in water, SBA was unable to be regenerated.

As was observed for SBA and SB(CF<sub>3</sub>COO<sup>-</sup>), SB(CCl<sub>3</sub>COO<sup>-</sup>) was also stable when stored under normal laboratory conditions for six months, as evidenced by no noteworthy changes in the PXRD and FTIR spectra (**Figure 7**). There was, however, an observed browning of the six-month-

old samples. This is likely the result of some of the silver cations of the CP forming silver metal or silver oxide. TGA data showed SB(CCl<sub>3</sub>COO<sup>-</sup>) undergoes multiple mass loss events when heated, with a decomposition onset temperature of *ca.* 90 °C (**Figure S9**). Variable temperature PXRD shows the changes in powder pattern for each major transition (**Figure S10**). The change in mass observed at 100 °C ( $\sim$  20 wt.%) results in a transition material that is stable until 165 °C. Upon further heating, the material continues to decompose until becoming amorphous by 550 °C. The peaks at  $2\theta \sim 38^\circ$  and  $43^\circ$  arise from the sample holder.

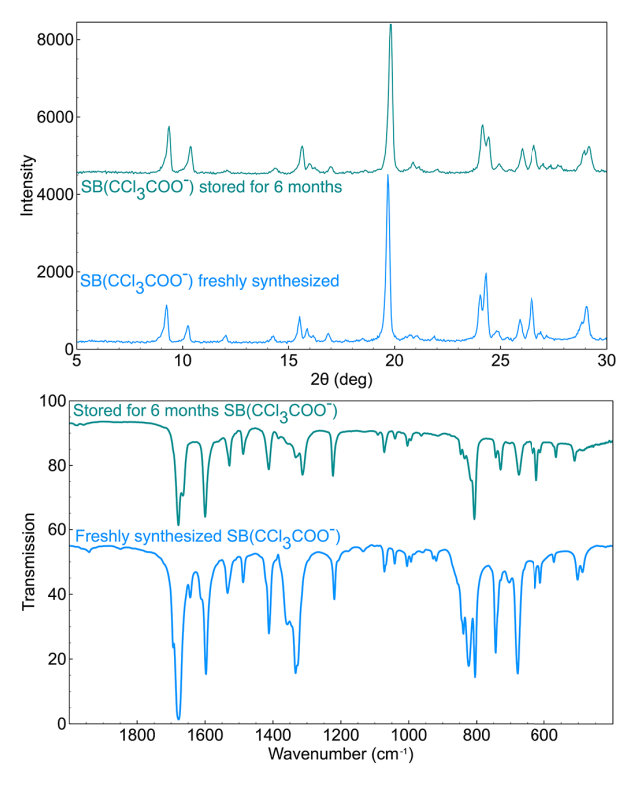


**Figure 7.** PXRD and FTIR (inset), showing that SB(CCl<sub>3</sub>COO<sup>-</sup>) is stable over the course of six months when stored in a vial under normal laboratory conditions.

## SBA Anion Exchange with CBr<sub>3</sub>COO<sup>-</sup>

The anions CF<sub>3</sub>COO<sup>-</sup> and CCl<sub>3</sub>COO<sup>-</sup> were successfully exchanged for the acetate of SBA to form the structurally similar CPs SB(CF<sub>3</sub>COO<sup>-</sup>) and SB(CCl<sub>3</sub>COO<sup>-</sup>). This was not the case, however, with CBr<sub>3</sub>COO<sup>-</sup>. Attempts to isolate single crystals of a CP structurally similar to the above frameworks that contained CBr<sub>3</sub>COO<sup>-</sup> were unsuccessful. A bulk material of unknown structure forms upon reaction of SBA with the anion CBr<sub>3</sub>COO<sup>-</sup> (optical micrograph, **Figure S11**). The theoretical PXRD pattern obtained from SCXRD data does not match the bulk product obtained from mixing SBA with CBr<sub>3</sub>COONa in an aqueous environment (**Figure 8**).

Various attempts were made at obtaining single crystals for a compound that matched the PXRD of the bulk product but all efforts resulted in single crystals suitable for SCXRD analysis that correspond to a new material belonging to space group *I*2 (**Figure 9**). This 1D CP consists of Ag<sup>+</sup> and 4,4'-bipyridine polymeric chains with bridging bromides and varies significantly from structures obtained through anion exchange of SBA with CF<sub>3</sub>COO<sup>-</sup> and CCl<sub>3</sub>COO<sup>-</sup> (ORTEP diagram **Figure S12**). The

CP consists of 4,4'-bipyridine linked through Ag-Ag dimers with a Ag...Ag distance of 3.0310(14) Å. These cations are ionically bound to µ3 bridging bromides with Ag-Br bond lengths ranging from 2.6174(18) Å to 2.8241(18) Å. Haloacetates are known to decompose to the corresponding halides with a stability trend of CF<sub>3</sub>COO<sup>-</sup> > CCl<sub>3</sub>COO<sup>-</sup> > CBr<sub>3</sub>COO<sup>-</sup>.<sup>44</sup> The source of bromide that incorporates itself into the structure [(Ag)(4,4'bipyridine) [Br] as the charge-balancing anion is therefore from the decomposition of CBr<sub>3</sub>COO<sup>-</sup>. Initially this structure was surprising since the Ag<sup>+</sup> present in the mixture didn't simply combine with Br to form highly water insoluble AgBr. The crystal structure, however, shows that AgBr chains formed with orthogonal coordinate bonds between Ag<sup>+</sup> and 4,4'-bipyridine, connecting the AgBr chains (Figure 9). This behavior offers insight into the interactions of halides in the presence of metals and organic linkers.

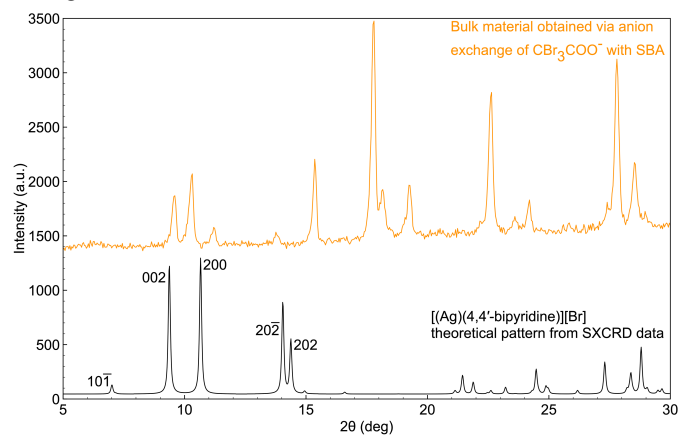


**Figure 8.** The experimental PXRD (top) does not match the theoretical PXRD of the compound produced from the combination of SBA and CBr<sub>3</sub>COONa in an aqueous environment (bottom), indicating the bulk product did not correspond to the structure obtained from the single crystals.

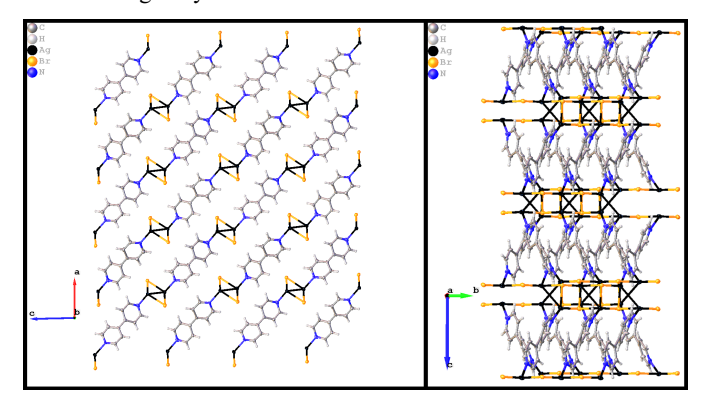


**Figure 9.** The structure of [(Ag)(4,4'-bipyridine)][Br], obtained from the reaction of SBA with CBr<sub>3</sub>COONa. The structure consists of AgBr chains extending along the *b*-axis. The chains are connected through orthogonal coordinate bonds between Ag<sup>+</sup> and 4,4'-bipyridine, seen here viewed along the *b*-axis (left) and *a*-axis (right).

## SBA Anion Exchange with CI<sub>3</sub>COO<sup>-</sup>

Finally, our investigation led us to explore the last member of the perhalogenated acetate anion family, CI<sub>3</sub>COO<sup>-</sup>. In contrast to prior materials, the combination of SBA with CI<sub>3</sub>COONa in an aqueous ambient setting resulted in a material

exhibiting a weak PXRD pattern that is inconsistent with a crystalline structure (**Figure 10**). We hypothesized that the larger size of iodine might hinder CI<sub>3</sub>COO<sup>-</sup> integration into a framework. Consequently, hydrothermal techniques were employed in an endeavor to produce a framework derived from CI<sub>3</sub>COO<sup>-</sup>. Aqueous SBA and CI<sub>3</sub>COONa were heated at 150 °C for 3 d under autogenous pressure. The resulting crystals exhibited a red-orange hue and PXRD analysis revealed three prominent higher angle peaks (**Figure 10**). The optical micrograph of the crystals is shown in **Figure S13**. The sample contained many crystals of SCXRD quality that were studied further.

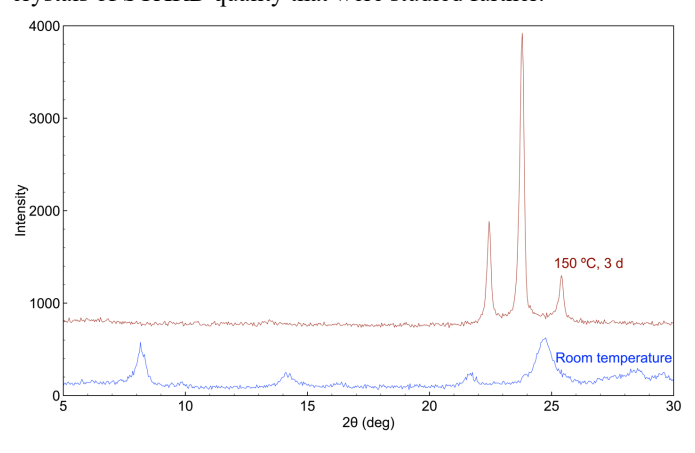


**Figure 10.** PXRD patterns of the bulk product obtained by combining SBA with CI<sub>3</sub>COONa in aqueous ambient conditions (blue, bottom) and at 150 °C under autogenous pressure (red, top).

SCXRD data revealed two unique hydrothermal products, neither of which matched the experimental PXRD of the bulk material. This implies the single crystals that were analyzed are likely minor byproducts of the reaction. The first analyzed is a novel compound consisting of Ag+, pyridine and I- $\{[(Ag)(C_5H_5N)][I]\}$  and belonging to space group  $P2_1/n$  (Figure 11). The material adopts pyridine into its structure that originates from the decomposition of the starting 4,4'-bipyridine (ORTEP diagram, Figure S14). As was observed for SB(CBr<sub>3</sub>COO<sup>-</sup>), this structure also contains a metal halide layer in addition to an interlamellar organic layer. AgI salt regions extend along the a-axis, with pyridine coordinated to Ag<sup>+</sup> and protruding from the layers orthogonally along the b-axis. Since the theoretical PXRD for this compound does not match that of the bulk product, [(Ag)(C5H5N)][I] is likely a minor side product of the reaction (Figure 12).

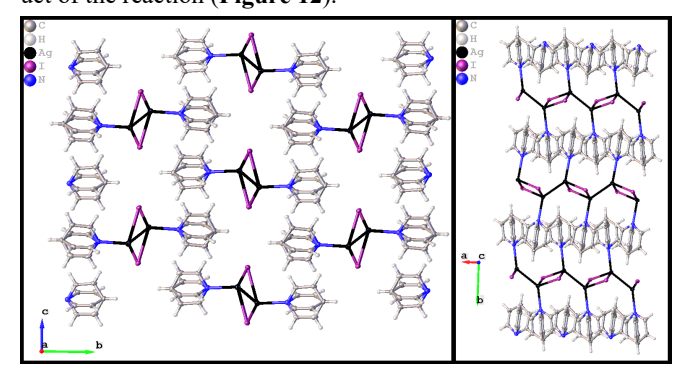


**Figure 11.** The crystal structure for  $[(Ag^+)(C_5H_5N)][I^-]$ , obtained by reacting SBA with CI<sub>3</sub>COONa at 150 °C for 3 d under autogenous pressure. Left image: view down the *a*-axis with AgI extending in and out of the page; right image: view down the *c*-axis with

AgI chains in the plane of the page. The capping pyridine molecules align with one another in a layered manner, shown here with disorder included.

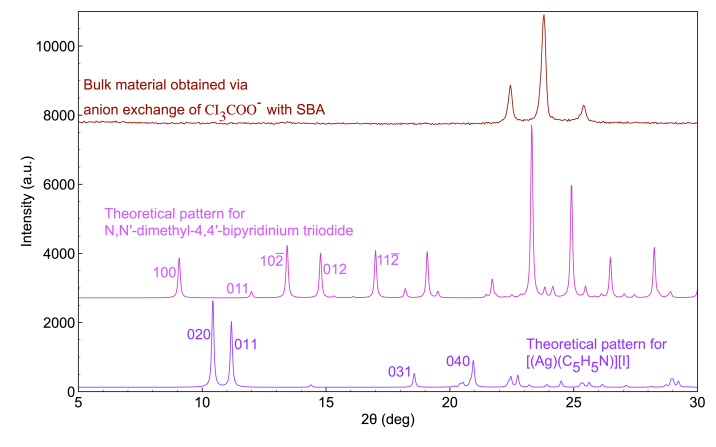


**Figure 12.** PXRD of the bulk material (top) and the theoretical patterns obtained from single crystal data for [(Ag)(C<sub>5</sub>H<sub>5</sub>N)][I] (center) and N,N'-dimethyl-4,4'-bipyridinium triiodide (bottom). The lack of a pattern match between the bulk product and the SCXRD data indicates the crystals selected were minor side products.

An additional compound was also collected from the bulk that matched a previously reported material belonging to space group  $P2_1/c$  (Figure 13).<sup>45</sup> This compound contained no extended coordinate bonds but was rather a salt consisting of N,N'-dimethyl-4,4'-bipyridinium and triiodide (ORTEP diagram, Figure S15). This material is the result of the dimethylation of the starting 4,4'-bipyridine and the liberation and combination of the iodine of the starting  $CI_3COO^-$  into triiodide. Like the previous compound, this material does not match the PXRD of the bulk solid collected and is an additional side product (Figure 12). All attempts to collect single crystals with a PXRD that matched the experimental pattern were unsuccessful.

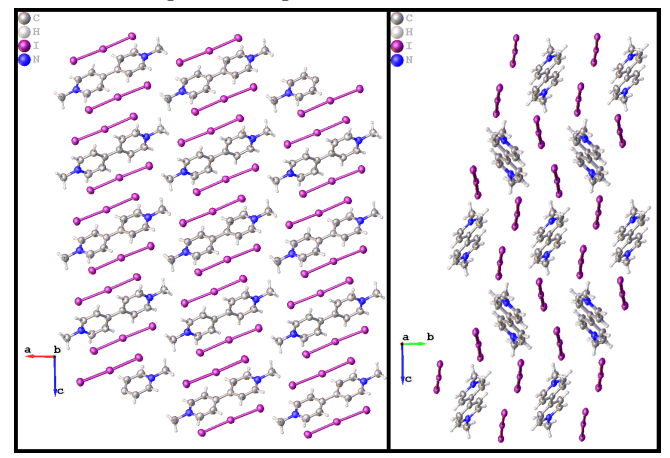


**Figure 13.** View along the *b*-axis (left) and *a*-axis (right) for the crystal structure of the salt N,N'-dimethyl-4,4'-bipyridinium triiodide, isolated from the hydrothermal reaction of SBA with CI<sub>3</sub>COONa.

## **CONCLUSIONS**

Our investigation focused on exploring the structural characteristics and stability of cationic metal-organic frameworks (CPs) formed by anion exchange reactions involving

perhalogenated acetate anions with frameworks composed of silver cations and 4,4'-bipyridine. Successful anion exchange reactions with SBA were observed for CF<sub>3</sub>COO<sup>-</sup> and CCl<sub>3</sub>COO<sup>-</sup>. The theoretical PXRD from SCXRD data matched the bulk material for both compounds. PXRD and FTIR were used to show the materials were stable over the course of six months when stored under normal laboratory conditions. When SBA is introduced to CBr<sub>3</sub>COO<sup>-</sup> or CI<sub>3</sub>COO<sup>-</sup>, no exchange product was observed using SCXRD but rather the anions underwent decomposition. These decomposed species were incorporated into the resulting material, contributing to the overall structural complexity. Our study sheds light on the efficacy of the initial CP, silver 4,4'-bipyridine acetate (SBA), in adsorbing perhalogenated pollutants from aqueous environments. The successful anion exchange reactions revealed the capability of SBA to adsorb CF<sub>3</sub>COO<sup>-</sup> and CCl<sub>3</sub>COO<sup>-</sup>, showcasing its potential for environmental remediation efforts. This work contributes to the growing field of metal-organic frameworks, especially cationic variants, and their potential applications in addressing environmental challenges posed by perhalogenated pollutants. It may be possible to also target some of the emerging, highly toxic longer chain analogs. The structural understanding gained from these experiments opens avenues for further research into the design and optimization of CPs for targeted environmental anion remediation.

#### ASSOCIATED CONTENT

### **Supporting Information**

The Supporting Information is available free of charge on the ACS Publications website. Crystallographic structural files for SLUG-59 to 62 and N,N'-dimethyl-4,4'-bipyridinium triiodide (CIF). Additional data and information (PDF): crystallographic tables, thermal ellipsoid plots, optical micrographs, FTIR spectra, TGA curves and VT-PXRD patterns.

## **Accession Codes**

CCDC 2349473, 2349474, 2349475 and 2349481 contain the supplementary crystallographic data for this paper. These data can be obtained free of charge via www.ccdc.cam.ac.uk/data\_request/cif, or by emailing data\_request@ccdc.cam.ac.uk, or by contacting The Cambridge Crystallographic Data Centre, 12 Union Road, Cambridge CB2 1EZ, UK; fax: +44 1223 336033.

#### **Author Information**

Scott R. J. Oliver - Department of Chemistry and Biochemistry, University of California Santa Cruz, Santa Cruz, California 95060, Unites States, <a href="http://orcid.org/0000-0002-6160-1518">http://orcid.org/0000-0002-6160-1518</a>; Email: <a href="mailto:soliver@ucsc.edu">soliver@ucsc.edu</a>

#### **Author Contributions**

The manuscript was written by KCL and SRJO. Experimentation was performed by KCL and KJF. Project conceptualization by KCL and JLB. SCXRD and structure refinements were performed by DGD and TCJ. Variable temperature PXRD was performed by JLB. All authors have given approval to the final version of the manuscript.

# **Funding Sources**

NSF-204469 and NSF-2018501.

#### Notes

The authors declare no competing financial interests.

## Acknowledgements

This work was supported in part by the National Science Foundation under grant No. 2044692. The single-crystal X-ray diffractometer housed in the UCSC X-ray Diffraction Facility was funded by NSF MRI grant no. 2018501.

#### **Abbreviations**

SBA: silver 4,4'-bipyridine acetate; SB(CF<sub>3</sub>COO<sup>-</sup>): silver 4,4'-bipyridine trifluoroacetate; SB(CCl<sub>3</sub>COO<sup>-</sup>): silver 4,4'-bipyridine trichloroacetate.

#### REFERENCES

- (1) Shen, N.; Yang, Z.; Liu, S.; Dai, X.; Xiao, C.; Taylor-Pashow, K.; Li, D.; Yang, C.; Li, J.; Zhang, Y.; Zhang, M.; Zhou, R.; Chai, Z.; Wang, S. 99TcO4– Removal from Legacy Defense Nuclear Waste by an Alkaline-Stable 2D Cationic Metal Organic Framework. *Nat. Commun.* 2020, 11 (1), 5571. https://doi.org/10.1038/s41467-020-19374-9.
- (2) Zhu, L.; Sheng, D.; Xu, C.; Dai, X.; Silver, M. A.; Li, J.; Li, P.; Wang, Y.; Wang, Y.; Chen, L.; Xiao, C.; Chen, J.; Zhou, R.; Zhang, C.; Farha, O. K.; Chai, Z.; Albrecht-Schmitt, T. E.; Wang, S. Identifying the Recognition Site for Selective Trapping of <sup>99</sup> TcO 4 <sup>-</sup> in a Hydrolytically Stable and Radiation Resistant Cationic Metal–Organic Framework. *J. Am. Chem. Soc.* 2017, 139 (42), 14873–14876. https://doi.org/10.1021/jacs.7b08632.
- (3) Andrews, D. Q.; Naidenko, O. V. Population-Wide Exposure to Per- and Polyfluoroalkyl Substances from Drinking Water in the United States. *Environ. Sci. Technol. Lett.* 2020, 7 (12), 931–936. https://doi.org/10.1021/acs.estlett.0c00713.
- (4) Pals, J. A.; Ang, J. K.; Wagner, E. D.; Plewa, M. J. Biological Mechanism for the Toxicity of Haloacetic Acid Drinking Water Disinfection Byproducts. *Environ. Sci. Technol.* 2011, 45 (13), 5791–5797. https://doi.org/10.1021/es2008159.
- (5) Lan, J.; Rahman, S. M.; Gou, N.; Jiang, T.; Plewa, M. J.; Alshawabkeh, A.; Gu, A. Z. Genotoxicity Assessment of Drinking Water Disinfection Byproducts by DNA Damage and Repair Pathway Profiling Analysis. *Environ. Sci. Technol.* 2018, 52 (11), 6565–6575. https://doi.org/10.1021/acs.est.7b06389.
- (6) Yang, X.; Shang, C.; Huang, J.-C. DBP Formation in Break-point Chlorination of Wastewater. Water Res. 2005, 39 (19), 4755–4767. https://doi.org/10.1016/j.watres.2005.08.033.
- (7) Liu, J.; Zhang, X.; Li, Y. Photoconversion of Chlorinated Saline Wastewater DBPs in Receiving Seawater Is Overall a Detoxification Process. *Environ. Sci. Technol.* 2017, 51 (1), 58–67. https://doi.org/10.1021/acs.est.6b04232.
- (8) Heller-Grossman, L.; Manka, J.; Limoni-Relis, B.; Rebhun, M. Formation and Distribution of Haloacetic Acids, THM and Tox in Chlorination of Bromide-Rich Lake Water. *Water Res.* 1993, 27 (8), 1323–1331. https://doi.org/10.1016/0043-1354(93)90219-8.
- (9) Liang, L.; Singer, P. C. Factors Influencing the Formation and Relative Distribution of Haloacetic Acids and Trihalomethanes in Drinking Water. *Environ. Sci. Technol.* 2003, 37 (13), 2920– 2928. https://doi.org/10.1021/es026230q.
- (10) Ashton, F. M.; Crafts, A. S. Mode of Action of Herbicides; Wiley: New York, 1973.
- (11) Lewis, T. E.; Wolfinger, T. F.; Barta, M. L. The Ecological Effects of Trichloroacetic Acid in the Environment. *Environ. Int.* 2004, 30 (8), 1119–1150. https://doi.org/10.1016/j.envint.2004.04.003.
- (12) Richardson, S. D.; Thruston, A. D.; Krasner, S. W.; Weinberg, H. S.; Miltner, R. J.; Schenck, K. M.; Narotsky, M. G.; McKague, A. B.; Simmons, J. E. Integrated Disinfection By-

- Products Mixtures Research: Comprehensive Characterization of Water Concentrates Prepared from Chlorinated and Ozonated/Postchlorinated Drinking Water. *J. Toxicol. Environ. Health A* **2008**, *71* (17), 1165–1186. https://doi.org/10.1080/15287390802182417.
- (13) Li, X.; Ma, J.; Liu, G.; Fang, J.; Yue, S.; Guan, Y.; Chen, L.; Liu, X. Efficient Reductive Dechlorination of Monochloroacetic Acid by Sulfite/UV Process. *Environ. Sci. Technol.* 2012, 46 (13), 7342–7349. https://doi.org/10.1021/es3008535.
- (14) Qian, Y.; Wang, W.; Boyd, J. M.; Wu, M.; Hrudey, S. E.; Li, X.-F. UV-Induced Transformation of Four Halobenzoquinones in Drinking Water. *Environ. Sci. Technol.* 2013, 47 (9), 4426– 4433. https://doi.org/10.1021/es305044k.
- (15) Mao, R.; Li, N.; Lan, H.; Zhao, X.; Liu, H.; Qu, J.; Sun, M. Dechlorination of Trichloroacetic Acid Using a Noble Metal-Free Graphene–Cu Foam Electrode via Direct Cathodic Reduction and Atomic H\*. Environ. Sci. Technol. 2016, 50 (7), 3829–3837. https://doi.org/10.1021/acs.est.5b05006.
- (16) Martin, E. T.; McGuire, C. M.; Mubarak, M. S.; Peters, D. G. Electroreductive Remediation of Halogenated Environmental Pollutants. *Chem. Rev.* 2016, 116 (24), 15198–15234. https://doi.org/10.1021/acs.chemrev.6b00531.
- (17) Almassi, S.; Samonte, P. R. V.; Li, Z.; Xu, W.; Chaplin, B. P. Mechanistic Investigation of Haloacetic Acid Reduction Using Carbon-Ti 4 O 7 Composite Reactive Electrochemical Membranes. *Environ. Sci. Technol.* 2020, 54 (3), 1982–1991. https://doi.org/10.1021/acs.est.9b06744.
- (18) Hozalski, R. M.; Zhang, L.; Arnold, W. A. Reduction of Haloacetic Acids by Fe  $^{0}$ : Implications for Treatment and Fate. *Environ. Sci. Technol.* **2001**, 35 (11), 2258–2263. https://doi.org/10.1021/es001785b.
- (19) Adhikary, J.; Meistelman, M.; Burg, A.; Shamir, D.; Meyerstein, D.; Albo, Y. Reductive Dehalogenation of Monobromo-and Tribromoacetic Acid by Sodium Borohydride Catalyzed by Gold Nanoparticles Entrapped in Sol–Gel Matrices Follows Different Pathways. Eur. J. Inorg. Chem. 2017, 2017 (11), 1510–1515. https://doi.org/10.1002/ejic.201700069.
- (20) Zhang, P.; LaPara, T. M.; Goslan, E. H.; Xie, Y.; Parsons, S. A.; Hozalski, R. M. Biodegradation of Haloacetic Acids by Bacterial Isolates and Enrichment Cultures from Drinking Water Systems. *Environ. Sci. Technol.* 2009, 43 (9), 3169–3175. https://doi.org/10.1021/es802990e.
- (21) Harding-Marjanovic, K. C.; Yi, S.; Weathers, T. S.; Sharp, J. O.; Sedlak, D. L.; Alvarez-Cohen, L. Effects of Aqueous Film-Forming Foams (AFFFs) on Trichloroethene (TCE) Dechlorination by a *Dehalococcoides Mccartyi* -Containing Microbial Community. *Environ. Sci. Technol.* 2016, 50 (7), 3352–3361. https://doi.org/10.1021/acs.est.5b04773.
- (22) Janssen, D. B.; Stucki, G. Perspectives of Genetically Engineered Microbes for Groundwater Bioremediation. *Environ. Sci. Process. Impacts* 2020, 22 (3), 487–499. https://doi.org/10.1039/C9EM00601J.
- (23) Russell, M. H.; Hoogeweg, G.; Webster, E. M.; Ellis, D. A.; Waterland, R. L.; Hoke, R. A. TFA from HFO-1234yf: Accumulation and Aquatic Risk in Terminal Water Bodies. *Environ. Toxicol. Chem.* 2012, 31 (9), 1957–1965. https://doi.org/10.1002/etc.1925.
- (24) Wu, J.; Martin, J. W.; Zhai, Z.; Lu, K.; Li, L.; Fang, X.; Jin, H.; Hu, J.; Zhang, J. Airborne Trifluoroacetic Acid and Its Fraction from the Degradation of HFC-134a in Beijing, China. *Environ.* Sci. Technol. 2014, 48 (7), 3675–3681. https://doi.org/10.1021/es4050264.
- (25) Zhai, Z.; Wu, J.; Hu, X.; Li, L.; Guo, J.; Zhang, B.; Hu, J.; Zhang, J. A 17-Fold Increase of Trifluoroacetic Acid in Landscape Waters of Beijing, China during the Last Decade. *Chem-osphere* 2015, 129, 110–117. https://doi.org/10.1016/j.chemosphere.2014.09.033.
- (26) Visscher, P. T.; Culbertson, C. W.; Oremland, R. S. Degradation of Trifluoroacetate in Oxic and Anoxic Sediments. *Nature* 1994, 369 (6483), 729–731. https://doi.org/10.1038/369729a0.

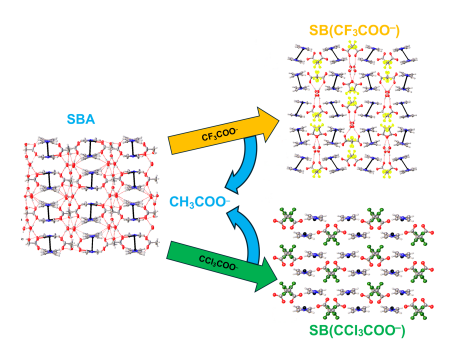
- (27) Berends, A. G.; Boutonnet, J. C.; Rooij, C. G. D.; Thompson, R. S. Toxicity of Trifluoroacetate to Aquatic Organisms. *Envi*ron. Toxicol. Chem. 1999, 18 (5), 1053–1059. https://doi.org/10.1002/etc.5620180533.
- (28) Ellis, D. A.; Hanson, M. L.; Sibley, P. K.; Shahid, T.; Fineberg, N. A.; Solomon, K. R.; Muir, D. C. G.; Mabury, S. A. The Fate and Persistence of Trifluoroacetic and Chloroacetic Acids in Pond Waters. *Chemosphere* 2001, 42 (3), 309–318. https://doi.org/10.1016/S0045-6535(00)00066-7.
- (29) Ellis, D. A.; Mabury, S. A.; Martin, J. W.; Muir, D. C. G. Thermolysis of Fluoropolymers as a Potential Source of Halogenated Organic Acids in the Environment. *Nature* 2001, 412 (6844), 321–324. https://doi.org/10.1038/35085548.
- (30) Xie, G.; Cui, J.; Zhai, Z.; Zhang, J. Distribution Characteristics of Trifluoroacetic Acid in the Environments Surrounding Fluorochemical Production Plants in Jinan, China. *Environ. Sci. Pollut. Res.* 2020, 27 (1), 983–991. https://doi.org/10.1007/s11356-019-06689-4.
- (31) Rigaku Oxford Diffraction CrysAlisPro Software System, Version 1.171.40.78a; Rigaku Corporation: Wroclaw, Poland, 2020.
- (32) Sheldrick, G. M. Crystal Structure Refinement with SHELXL. Acta Crystallogr. Sect. C Struct. Chem. 2015, 71 (1), 3–8. https://doi.org/10.1107/S2053229614024218.
- (33) Dolomanov, O. V.; Bourhis, L. J.; Gildea, R. J.; Howard, J. A. K.; Puschmann, H. *OLEX2*: A Complete Structure Solution, Refinement and Analysis Program. *J. Appl. Crystallogr.* 2009, 42 (2), 339–341. https://doi.org/10.1107/S0021889808042726.
- (34) Müller, P. Practical Suggestions for Better Crystal Structures. *Crystallogr. Rev.* **2009**, *15* (1), 57–83. https://doi.org/10.1080/08893110802547240.
- (35) Citrak, S. C.; Popple, D.; Delgado-Cunningham, K.; Tabler, K.; Bdeir, K.; Oliver, A. G.; Kvam, P. B.; Oliver, S. R. J. Extremely Rapid Uptake of Perchlorate with Release of an Environmentally Benign Anion: Silver Bipyridine Acetate. *Cryst. Growth Des.* 2018, 18 (3), 1891–1895. https://doi.org/10.1021/acs.cgd.7b01797.
- (36) Citrak, S. C.; Bdeir, K.; Delgado-Cunningham, K.; Popple, D.; Oliver, S. R. J. Exchange Capability of Cationic Silver 4,4'-Bipyrdine Materials for Potential Water Remediation: Structure, Stability, and Anion Exchange Properties. *Inorg. Chem.* 2019, 58 (11), 7189–7199. https://doi.org/10.1021/acs.inorgchem.9b00115.
- (37) Fang, Q.; Zhu, G.; Xue, M.; Wang, Z.; Sun, J.; Qiu, S. Amine-Templated Assembly of Metal–Organic Frameworks with Attractive Topologies. *Cryst. Growth Des.* 2008, 8 (1), 319–329. https://doi.org/10.1021/cg070604f.
- (38) Xu, G.-C.; Ding, Y.-J.; Okamura, T.; Huang, Y.-Q.; Bai, Z.-S.; Hua, Q.; Liu, G.-X.; Sun, W.-Y.; Ueyama, N. CPs with Varied Metal Centers and Flexible Tripodal Ligand 1,3,5-Tris(Imidazol-1-Ylmethyl)Benzene: Synthesis, Structure, and Reversible Anion Exchange Property. Cryst. Growth Des. 2009, 9 (1), 395–403. https://doi.org/10.1021/cg800600g.
- (39) Michaelides, A.; Skoulika, S. Anion-Induced Formation of Lanthanide-Organic Chains From 3D Framework Solids. Anion Exchange in a Crystal-to-Crystal Manner. Cryst. Growth Des. 2009, 9 (5), 2039–2042. https://doi.org/10.1021/cg801138e.
- (40) Cui, X.; Khlobystov, A. N.; Chen, X.; Marsh, D. H.; Blake, A. J.; Lewis, W.; Champness, N. R.; Roberts, C. J.; Schröder, M. Dynamic Equilibria in Solvent-Mediated Anion, Cation and Ligand Exchange in Transition-Metal CPs: Solid-State Transfer or Recrystallisation? *Chem. Eur. J.* 2009, 15 (35), 8861–8873. https://doi.org/10.1002/chem.200900796.
- (41) Van Der Sluys, W. G. The Solubility Rules: Why Are All Acetates Soluble? *J. Chem. Educ.* **2001**, 78 (1), 111. https://doi.org/10.1021/ed078p111.
- (42) Wu, Y.-C.; Friedman, H. L. Heats of Solution of Some Trifluoroacetates, Tetraphenylborates, Iodides, and Perchlorates in Water and in Propylene Carbonate and the Relative Enthalpies of Solvation of the Alkali Metal Ions in Propylene Carbonate.

- *J. Phys. Chem.* **1966**, 70 (2), 501–509. https://doi.org/10.1021/j100874a030.
- (43) Walker, M. A. Improvement in Aqueous Solubility Achieved via Small Molecular Changes. *Bioorg. Med. Chem. Lett.* **2017**, 27 (23), 5100–5108. https://doi.org/10.1016/j.bmcl.2017.09.041
- https://doi.org/10.1016/j.bmcl.2017.09.041.
  (44) Lifongo, L. L.; Bowden, D. J.; Brimblecombe, P. Thermal Degradation of Haloacetic Acids in Water. *Int J Phys Sci* 10.
- (45) García, M. D.; Martí-Rujas, J.; Metrangolo, P.; Peinador, C.; Pilati, T.; Resnati, G.; Terraneo, G.; Ursini, M. Dimensional Caging of Polyiodides: Cation-Templated Synthesis Using Bipyridinium Salts. CrystEngComm 2011, 13 (13), 4411. https://doi.org/10.1039/c0ce00860e.

# Perhalogenated Anions as Structure Directing Agents of Cationic Coordination Polymers

Kevin C. Lofgren, Kellii J. Fusari, Daniel G. Droege, Jeremy L. Barnett, Timothy C. Johnstone and Scott R. J. Oliver\*

# **TOC GRAPHIC**



# TOC SYNOPSIS

We studied the effects of using the perhalogenated acetate anions trifluoro-, trichloro-, tribromo- and triiodoacetate for anion exchange reactions with the cationic metal-organic framework, silver 4,4'-bipyridine acetate for potential environmental remediation of halogenated pollutants.